Soft Matter

Cite this: *Soft Matter*, 2011, **7**, 11177

www.rsc.org/softmatter

PAPER

Hydrodynamic Rayleigh-Taylor-like instabilities in sedimenting colloidal mixtures

Kristina Milinković,*[a] Johan T. Padding[b] and Marjolein Dijkstra*[a]

Received 19th May 2011, Accepted 19th September 2011
DOI: 10.1039/c1sm05930k

We study the sedimentation of an initially inhomogeneous distribution of binary colloidal mixtures confined to a slit using a coarse-grained hybrid molecular dynamics and stochastic rotation dynamics simulation technique. This technique allows us to take into account the Brownian motion and hydrodynamic interactions between colloidal particles in suspensions. The sedimentation of such systems results in the formation of Rayleigh-Taylor-like hydrodynamic instabilities, and here we examine both the process of the formation and the evolution of the instability, as well as the structural organization of the colloids, depending on the properties of the binary mixture. We find that the structural properties of the swirls that form as a consequence of the instability depend greatly on the relative magnitudes of the Peclet numbers, and much less on the composition of the mixture. We also calculate the spatial colloid velocity correlation functions which allow us to follow the time evolution of the instability and the time dependence of the characteristic correlation length. Finally, we calculate the growth rates of the unstable modes both directly from our simulation data, and also using a theoretical approach, finding good agreement.

1 Introduction

Binary mixtures of colloidal particles exhibit a surprisingly rich phase behavior, with a wide diversity of binary crystal structures which have been extensively studied both by experiments and computer simulations (for a review see, for example, ref. 1). Depending on the properties of the constituting particles and the structures they form, these systems can both have fundamentally interesting properties *and* be useful for the development and fabrication of advanced materials, such as photonic crystals.[2] Photonic crystals are materials that do not allow light propagation in all directions and are therefore potentially suitable for applications related to controlling and manipulating the propagation of light. Experimental realization of these structures on optical scales, however, is still a challenge. The two colloidal crystal structures that would potentially have a large band gap in the visible region are the diamond[3,4] and pyrochlore[5,6] structures, which are the underlying lattices of one of the binary Laves phases.[7] This inspired a recently proposed fabrication method that involved using external fields to facilitate the self-assembly of a hard sphere binary Laves phase, followed by burning or dissolving of one of the colloidal species which would result in the desired structure.[8] The stability of these binary crystalline structures in hard-sphere mixtures has been investigated using computer simulations, where Gibbs free energy calculations showed that for diameter ratios in the range of $0.74 \leq q \leq 0.84$ Laves phases are stable.[8,9] However, while Laves phases have been so far experimentally observed in nanoparticle systems[10] and some colloidal systems,[11,12] they have not yet been fabricated for micro-meter-sized hard-sphere mixtures. The main issue lies in the fact that for micro-meter-sized colloids, which would be needed for obtaining a band gap in the visible region, gravity and slow crystallization rates hinder the formation of binary crystals.[13] With photonic applications in mind, fabrication of a binary Laves phase was attempted through the sedimentation of colloids[14] and it was observed that sedimentation starting from a vertically inhomogeneous distribution of particles (*i.e.* particles arranged on the upper capillary wall) leads to the development of inhomogeneities in the plane perpendicular to the gravitational field. The experiments also showed that when the sediment formed on the bottom wall, instead of forming the desired binary crystal structure, the particles of different species had become separated. However, whether this separation was a direct consequence of the observed horizontal density inhomogeneities is unclear, and it would therefore be desirable to study this process at the particle level.

In order to investigate the interplay between mixing and separation we simulate the sedimentation of binary colloidal systems immersed in a solvent and confined to a slit. The simulations start by mimicking a frequently used experimental

[a]*Soft Condensed Matter, Debye Institute for Nanomaterials Science, Utrecht University, Princetonplein 5, 3584 CC Utrecht, The Netherlands. E-mail: k.milinkovic@uu.nl; m.dijkstra1@uu.nl*
[b]*Department of Chemical Engineering and Chemistry, Eindhoven University of Technology, P.O. Box 513, 5600 MB Eindhoven, The Netherlands*

setup - an initially homogenized dispersion is left to sediment to the bottom of the slit so that when the sediment is equilibrated, the slit is turned upside down leaving a heavy colloid-fluid layer superimposed on top of a lighter one. Sedimentation of a configuration obtained in this way is accompanied by the formation of strong inhomogeneities, inducing lateral pattern formation, which resemble the hydrodynamic Rayleigh-Taylor instability. Instabilities arising due to unstable density distributions have been previously studied in different contexts.[15–17] For a one-component system of sterically-stabilized spherical colloids sedimenting in a slit, experimental observations of the Rayleigh-Taylor instability have been reported previously by Royall *et al.*,[18] and have also been studied *via* computer simulations by Padding and Louis[19] and Wysocki *et al.*,[20,21] who modeled the colloids as hard spheres.

The classic Rayleigh-Taylor instability occurs if a layer of a heavy fluid is placed on top of a lighter one.[22] The system will tend to minimize its potential energy, *i.e.* to reverse the positions of the fluids and during this process the interface that separates them will start to fluctuate. The growth of the unstable fluctuations results in the formation of the Rayleigh-Taylor instability.

The formation of the instability is driven by the gravitational field, and in our simulations the strength of the field acting on particles is characterized by their Peclet numbers. These numbers can be chosen independently for each of the species in the binary mixture. The limit in which $Pe \gg 1$ marks the granular domain where the effects of diffusion are small, while for $Pe \ll 1$, which is the case for relatively small colloids, diffusion dominates. In ref. 23 Padding and Louis showed that for steady state sedimentation and intermediate values of Pe numbers ($Pe = 0.1$–15) the average sedimentation velocity of hard-spheres is completely dominated by the hydrodynamic interactions and depends little on the exact value of the Peclet number. When simulating instabilities, which occur in non-equilibrium, along with Brownian fluctuations, computer simulations need to properly include hydrodynamic interactions mediated by the solvent.[24]

The simulation technique that we use in our study, since it captures both of these effects, is a coarse-grained hybrid molecular dynamics (MD) and stochastic rotation dynamics (SRD) scheme. It was first introduced by Malevanets and Kapral,[25] and previously used to study colloids,[23,26–29] polymers[30–32] and vesicles and cells.[33–35] As mentioned above, it has also been used to simulate the Rayleigh-Taylor-like instability of a one-component colloidal system in ref. 19–21.

Our goal in this work is to gain a detailed insight into how the properties of binary mixtures and their constituting particles influence the formation and the time development of the Rayleigh-Taylor-like instabilities, and to investigate the potential for controlling the organization of particle species during the sedimentation.

2 Model

Bridging the different time and length scales between colloidal particles and a solvent in computer simulations requires coarse-graining. To this end, we employ stochastic rotation dynamics to describe the hydrodynamic interactions between colloids mediated by a solvent. Below we briefly outline the method and refer the interested reader to ref. 36 for more technical details and also a discussion of other simulation techniques designed to describe the dynamics of colloidal suspensions.

SRD is a coarse-graining scheme that models the solvent as a large number, N_f, of point-like fluid particles each of mass m_f, free to move in continuous space with continuous velocities. The system, *i.e.* the simulation box, is coarse-grained into cubic cells of size a_0 so that when the fluid particles interact they do so only with the members of their own cell. There is no restriction on the number of fluid particles in a cell.

The dynamics of the solvent is conducted in two steps: streaming and collision. In the streaming step we integrate Newton's equations of motion for a time Δt_c. The forces acting on fluid particles are external and are generated by the colloids, gravity and the walls.

In the collision step, particles are sorted into cubic cells and their velocities relative to the center of mass velocity $\mathbf{v}_{cm}$ of the cell they belong to are rotated, *i.e*

$$\mathbf{v}_i \mapsto \mathbf{v}_{cm} + \mathbf{R}(\mathbf{v}_i - \mathbf{v}_{cm}), \tag{1}$$

where $\mathbf{v}_i$ is the velocity of the fluid particle i, and $\mathbf{R}$ is a rotation matrix that rotates the relative velocities by a fixed angle α about a random axis. We chose $\alpha = \pi/2$ for all our simulations. The purpose of the collision step is to allow the solvent particles to exchange momenta while conserving mass, momentum and kinetic energy in the cell. The transformation we describe does indeed conserve these properties, leading to correct hydrodynamics.[25] To ensure Galilean invariance, we include a grid shift procedure that shifts the fluid particles by a random vector before performing the collision step.[37]

Hard-sphere-like colloids are propagated through a molecular dynamics scheme and their coupling to the SRD bath is carried out *via* a repulsive interaction potential of the Weeks-Chandler-Andersen form

$$\phi_{fi}(r) = \begin{cases} 4\varepsilon\left[\left(\frac{\sigma_{fi}}{r}\right)^{12} - \left(\frac{\sigma_{fi}}{r}\right)^{6} + \frac{1}{4}\right] & \left(r \le 2^{1/6}\sigma_{fi}\right), \\ 0 & \left(r > 2^{1/6}\sigma_{fi}\right), \end{cases} \tag{2}$$

where $i = A, B$ denotes the colloidal species A or B, f denotes the solvent (fluid) particles and σ_{fi} is the colloid-fluid interaction range for species i.

The interaction between the colloids is represented by a similar, but steeper potential which takes the form

$$\phi_{ij}(r) = \begin{cases} 4\varepsilon\left[\left(\frac{\sigma_{ij}}{r}\right)^{48} - \left(\frac{\sigma_{ij}}{r}\right)^{24} + \frac{1}{4}\right] & \left(r \le 2^{1/24}\sigma_{ij}\right), \\ 0 & \left(r > 2^{1/24}\sigma_{ij}\right), \end{cases} \tag{3}$$

where $i, j = A, B$ and σ_{ij} is the colloid-colloid interaction range between species i and j. The colloid-fluid and colloid-colloid energy scales are set by ε. We integrate colloid-fluid and colloid-colloid forces using a velocity Verlet algorithm[38] with time step $\Delta t_{MD} = \Delta t_c/4$.

The number of fluid particles is much larger than the number of colloids, which can lead to the appearance of unwanted depletion forces between the colloids. Even a slight overlap between two colloids introduces strong attractions. In order to avoid this, we set particle diameters σ_{AA} and σ_{BB} to values larger than $2\sigma_{fA}$ and $2\sigma_{fB}$ respectively, and introduce an additional depletion compensating potential between the colloids to deal with the rare

cases when they are closer then $2\sigma_{fi}$ ($i = A, B$). For purely hard-sphere interactions the depletion potential can be calculated analytically. However, the repulsive interactions given in eqn (2) and (3) are slightly softer. The depletion force F_d arising due to these potentials has been calculated numerically by Padding and Louis who found that it fits well with a slightly altered form of the hard-sphere result.[36] The compensating force F_c is given by $F_c(r) = -F_d(r) = n_f k_B T \sigma_{fi}^2 0.85\left[4 - (r/(1.05\sigma_{fi}))^2\right]$, where r is the distance between two colloids, n_f is the number density of fluid particles, and we take $k_B T$ to be 1. The compensating potential acts for particle separations $r < 2.1\sigma_{fi}$.

Finally, since the system we simulate is out of equilibrium we need to couple it to a thermostat to keep the temperature constant. We do this by defining a global temperature based on the mean square deviations of the fluid particle velocities from their respective center of mass velocities of the cells they belong to. We measure the global temperature every Δt_c and then rescale the relative fluid particle velocities to get the correct temperature.[36]

3 Results

We consider binary mixtures of small and large hard-sphere like colloidal particles with diameters σ_{fA} and σ_{fB}, where $\sigma_{fA}/\sigma_{fB} = 0.83$. We choose this particle diameter ratio as it is close to the size ratio of particles forming a binary Laves phase with the highest packing fraction.[9] The mixtures we study have two different compositions. One consists of $N_A = 6500$ and $N_B = 3250$ colloids forming a system with twice as many small particles as large ones (which is the particle number ratio of a binary Laves phase) and in this case the volume fractions of the two species are roughly equal. The other mixture consists of $N_A = N_B = 6500$ colloidal particles. In both cases the colloids are immersed in a bath of $N_f \sim 15 \times 10^6$ solvent particles. The particles are confined between two walls in xy planes and we impose periodic boundary conditions in the x and y directions with gravity acting in the z direction. The dimensions of the slit are $L_z = 72a_0$, $L_x = L_y = 216a_0$ (giving $L_z = 14\sigma_{BB}$, $L_x = L_y = 42\sigma_{BB}$ or $L_z = 17\sigma_{AA}$, $L_x = L_y = 51\sigma_{AA}$) which are close to the dimensions of the experimental setup for a one-component system presented in ref. 21. The average number of fluid particles per SRD cell was set to $\gamma = 5$.

We characterize the motion of a colloid by the Peclet number, $Pe = \tau_D/t_S$, which is the ratio between the time τ_D a particle needs to diffuse over its own radius a, and the Stokes time, t_S, it needs to sediment over the same distance

$$t_S = \frac{a}{v_S}, \tag{4}$$

where v_S is the flow velocity. The Peclet number can be calculated as

$$Pe = \frac{M_b g a}{k_B T} = \frac{4\pi}{3}\frac{(\rho_c - \rho_f) g a^4}{k_B T}, \tag{5}$$

where M_b denotes the buoyant mass of a particle, $M_b = \frac{4}{3}\pi(\rho_c - \rho_f)a^3$, ρ_c and ρ_f are the mass densities of the colloids and the fluid respectively, g denotes the gravitational constant and a the effective hydrodynamic radius of the particle, determining the characteristic length scale.[36] A detailed discussion on how to map the parameters of our simulation method onto physical systems is given in ref. 36. For each system that we study we set the Peclet numbers of each of the species, Pe_A and Pe_B, independently and by doing so we determine the strength of the gravitational field and the masses of the particles. We have chosen to keep Pe_B at 12 and vary Pe_A by setting it to 6, 9, 12, 15 and 18. We note that as the particles in this study have fixed sizes, the relative Peclet number Pe_A/Pe_B, is proportional to the ratio of the effective mass densities of the two particle species $(\rho_A - \rho_f)/(\rho_B - \rho_f)$.

3.1 Rayleigh-Taylor-like instability

We let an initially homogeneous distribution of colloids confined to a slit sediment towards one wall until they reach an equilibrium distribution. This is checked by monitoring colloidal density profiles in time. Once the particles have settled at the bottom wall of the simulation box we invert the direction of gravity creating conditions suitable for the instability to develop. We let the system evolve further and, as a consequence of the instability, droplets of colloidal material form and sediment quickly towards the bottom wall. In this section we examine the structural properties of these droplets and their dependence on the composition of the mixture and the properties of the colloidal particles - specifically the Peclet numbers.

Fig. 1 shows the evolution of the systems with $N_A = 2N_B$ (Fig. 1, left column) and $N_A = N_B$ particles (Fig. 1, right column) and Peclet numbers $Pe_A = Pe_B = 12$, in the gravity plane. We see that the process of sedimentation is accompanied by the formation of swirls. Initially, the interface separating the colloid-rich region from the pure solvent region is almost flat, then

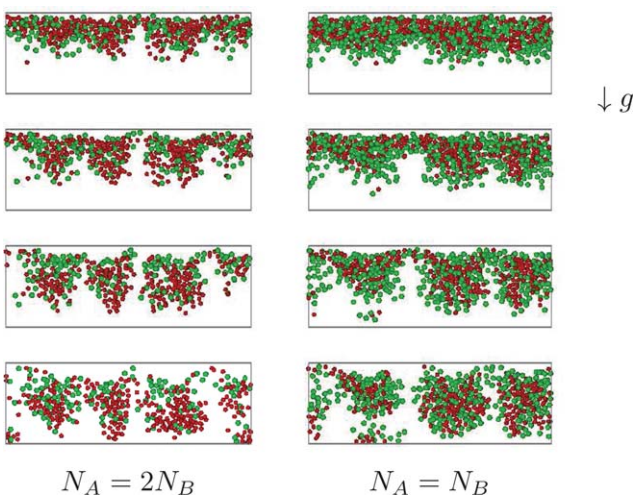

Fig. 1 Simulation snapshots of the time evolution (from top to bottom) of the Rayleigh-Taylor-like instability in binary mixtures of hard-sphere-like colloids with size ratio $\sigma_{fA}/\sigma_{fB} = 0.83$. Mixtures consist of $N_A = 2N_B$ (left column) and $N_A = N_B$ (right column) colloids with the same Peclet numbers $Pe_A = Pe_B = 12$. The snapshots are slices of thickness $2\sigma_{BB}$ in the vertical (xz) plane in the middle of the simulation box; gravity acts in the direction indicated in the figure (z direction). Particles belonging to species A (smaller) are colored red and particles belonging to species B (larger) are green.

undulations start to form and as their amplitude grows the colloidal layer resolves itself into droplets. This is a consequence of the instability - it facilitates the fluid back-flow and the transition of the system to a stable configuration *via* the instability. We note that the swirls we can see in Fig. 1 are very similar to those observed for a one-component system in ref. 19–21.

The added complexity of a binary mixture, however, provides for the possibility of different arrangements of colloidal particles of different species within the droplets themselves. In Fig. 2 we show the mass density profiles of each of the particle species as well as the overall colloidal mass density profile. We plot these against the height of the simulation box, at the start of the sedimentation process (Fig. 2a, 2b), at a time when the instability is fully developed (Fig. 2e, 2f) and a time in between the two (Fig. 2c, 2d). Comparing Fig. 2a and Fig. 2b we can see that initially the overall mass density profiles are not, qualitatively, significantly different. However, we do observe significant differences between the mixtures if we look at the distributions of individual species within the simulation box. While the shape of the distributions in the case when the Peclet number of smaller particles is smaller indicate a degree of mixing (Fig. 2a), when the Peclet number of smaller particles is larger we can clearly distinguish between two layers - one composed of heavier particles near the wall and one with lighter ones further away (Fig. 2b). At later times we again see that for the mixture in which the smaller particles are lighter (Fig. 2c, 2e) the relative density of the particle species, and hence the number ratio as well, is similar at all heights. This would lead us to expect much more evenly mixed samples in this case then in the case when the smaller particles are heavier (Fig. 2d, 2f) where we expect different degrees of mixing as a function of height. Clearly, depending on the relative magnitudes of the Peclet numbers the distributions of the colloidal particles will progress in different ways within the instability.

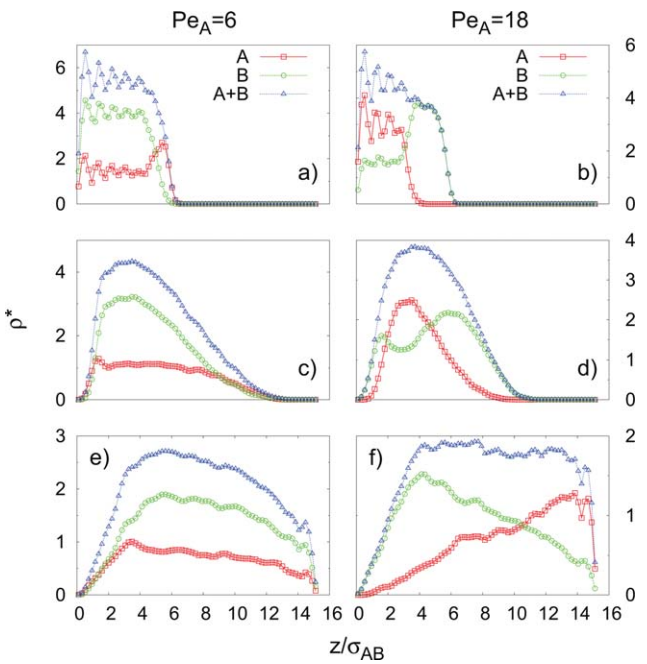

Fig. 2 Colloidal density profiles as a function of height of the simulation box at three different times, increasing from top to bottom; top corresponds to initial times, bottom to times when the instability is fully developed. Plots shown here correspond to mixtures with $N_A = N_B$, larger particles with $Pe_B = 12$ fixed and smaller with: $Pe_A = 6$ for the plots in the left column (species A is lighter in this case) and $Pe_A = 18$ for the plots in the right column (species A is heavier). Reduced mass density ρ^* is given as $\rho^* = \rho(a_0^3/m_f)$. Distances are rescaled by $\sigma_{AB} = (\sigma_{fA} + \sigma_{fB})/2$.

To examine the behavior within the horizontal planes, we present in Fig. 3 a series of simulation snapshots of a slice of the simulation box in the plane perpendicular to the direction of gravity, as the instability develops in time. Fig. 3 allows us to look closer at the time development of network-like structures that appear as a consequence of the Rayleigh-Taylor-like instability. The snapshots shown correspond to the systems with $N_A = 2N_B$ (Fig. 3a, 3b) and $N_A = N_B$ particles (Fig. 3c, 3d), and with Peclet numbers $Pe_B = 12$ and $Pe_A = 6$ and 18, *i.e.* $Pe_A = 0.5Pe_B$ and $Pe_A = 1.5Pe_B$, with those corresponding to times when the swirls are fully developed highlighted.

If we compare the highlighted snapshots in Fig. 3a and Fig. 3b, or the highlighted snapshots in Fig. 3c and Fig. 3d, corresponding to systems with the same particle number ratios but different relative Peclet numbers, we can see considerable differences in the structures formed. Although there is not much difference in the characteristic dimensions of the colloid-rich regions corresponding to the network branches (assuming the same particle number ratio), the distributions of particles of different species within the branches are different. In the case when the Peclet number of the smaller species is smaller (Fig. 3a compared to Fig. 3b, or Fig. 3c compared to Fig. 3d) the colloid-rich regions appear to be composed of similar numbers of A and B particles, randomly and homogeneously scattered throughout each region. However, in the case when the Peclet number of the smaller species is larger, we see that the smaller, heavier colloids are positioned mostly in the inner parts of the colloid-rich regions, with the larger particles positioned more towards the boundaries of these regions. As this organization of particles can be seen in both mixtures, *i.e.* mixtures with different number ratios of colloidal particles, we conclude that it must be due to gravitational effects, and not the composition of the mixture.

Additionally, we also observe from Fig. 3d that when the smaller particles are heavier, the Rayleigh-Taylor instability is initiated by the lighter colloid species B, and that at later times the heavier species A takes over as they sediment faster, leaving a layer of species B behind after the instability has fully developed. This visually demonstrates the behavior we see in the right column of Fig. 2.

In order to quantitatively describe the structures we see in the simulation snapshots in Fig. 3 we calculate the radial distribution functions $g_{ii}(r)$, $i = A, B$, in a slab of thickness $2\sigma_{BB}$ within the middle plane at a time when the instabilities have fully developed. In Fig. 4 we show the radial distribution functions for the systems with Peclet numbers $Pe_A = 6$ and $Pe_A = 18$, since these are the two extremes of the parameter range we have studied. We can see that the radial distribution functions calculated for the two mixtures do not depend strongly on the composition (compare Fig. 4a and Fig. 4c or Fig. 4b and Fig. 4d), but do show different behavior with different Pe_A. In the case where $Pe_A = 6$ both $g_{AA}(r)$ and $g_{BB}(r)$ curves exhibit second peaks, which for the larger species (B) are slightly more pronounced, and for the smaller species (A) are positioned at distances slightly larger than

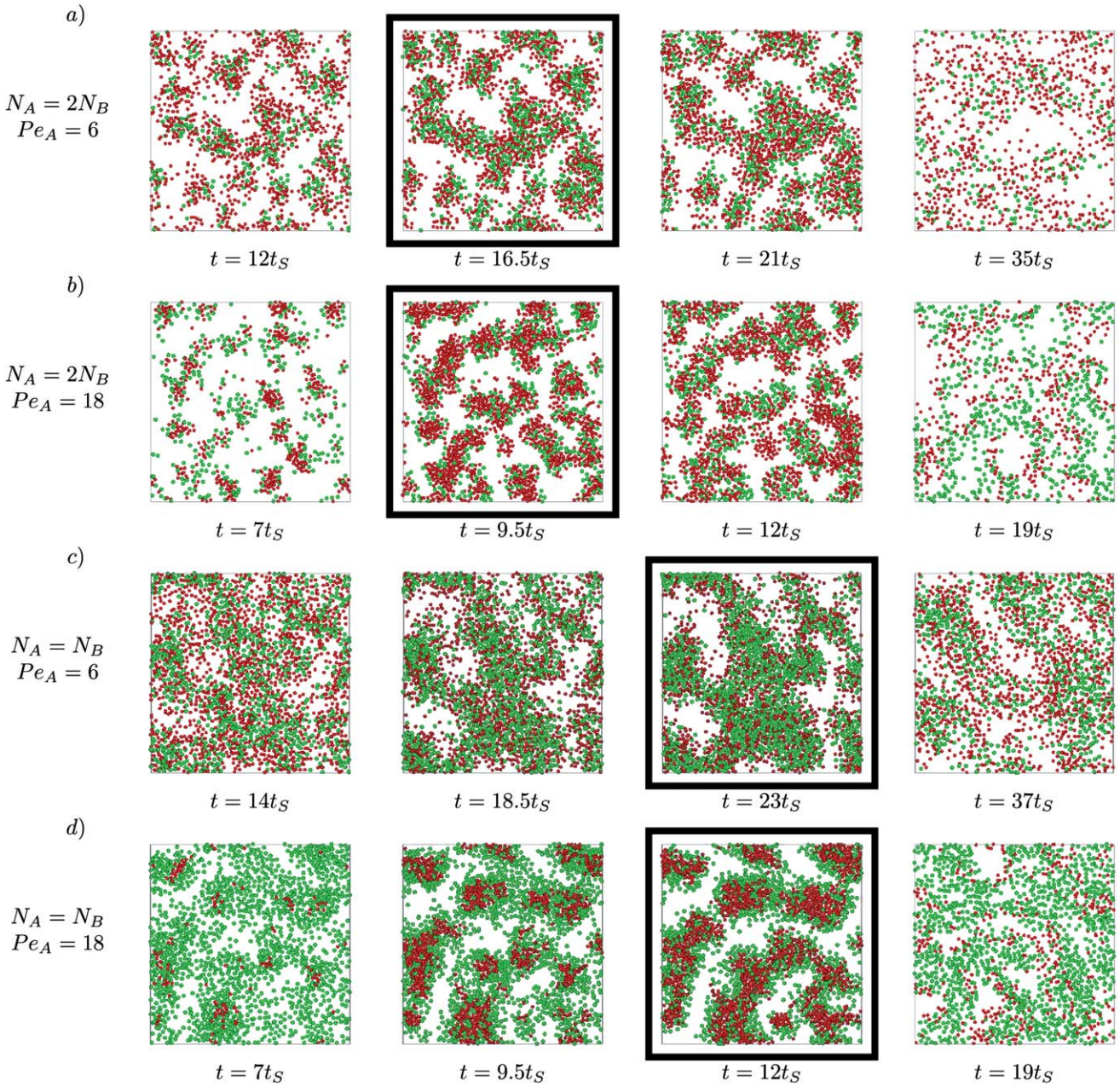

Fig. 3 Simulation snapshots of the time evolution (from left to right) of binary mixtures of hard-sphere-like colloids with size ratio $\sigma_{fA}/\sigma_{fB} = 0.83$, particle numbers N_A and N_B, Peclet numbers $Pe_B = 12$ and $Pe_A = 6$ and $Pe_A = 18$: a) $N_A = 2N_B$, $Pe_A = 6$; b) $N_A = 2N_B$, $Pe_A = 18$; c) $N_A = N_B$, $Pe_A = 6$; d) $N_A = N_B$, $Pe_A = 18$. The snapshots are slices of thickness $2\sigma_{BB}$ in the xy plane in the middle of the simulation box; gravity acts in the z direction. The time is measured in units of the Stokes time t_S of the larger species. Particles belonging to species A (smaller) are colored red and particles belonging to species B (larger) are green. Highlighted snapshots correspond to times when the swirls are fully developed.

$r = 2\sigma_{AA}$. In the case where $Pe_A = 18$, the curves corresponding to $g_{BB}(r)$ no longer exhibit a second peak which suggests a larger degree of dilution of species B compared to the $Pe_A = 6$ case. The plots of the radial distribution functions of the smaller particles, $g_{AA}(r)$ with $Pe_A = 18$ show for both mixtures very pronounced second peaks, which are positioned at $r \sim 2\sigma_{AA}$, and for the mixture with $N_A = N_B$ also a very small third peak at an even larger distance (Fig. 4d).

In summary, from Fig. 3 and 4 we conclude that the structure of the Rayleigh-Taylor-like instability is hardly affected by the composition of the binary mixture, but does strongly depend on the relative Peclet numbers of the two species. When the smaller colloids are lighter than the larger ones ($Pe_A < Pe_B$) the density profiles indicate a higher degree of mixing within the colloidal material than for the mixtures when the smaller colloids are heavier ($Pe_A > Pe_B$). We would expect that, without obstacles, the heavier colloidal species would sediment faster than the lighter species, and therefore we would expect to see separation of colloids whenever there is a sufficient difference in colloidal densities. However, larger particles will inevitably meet more

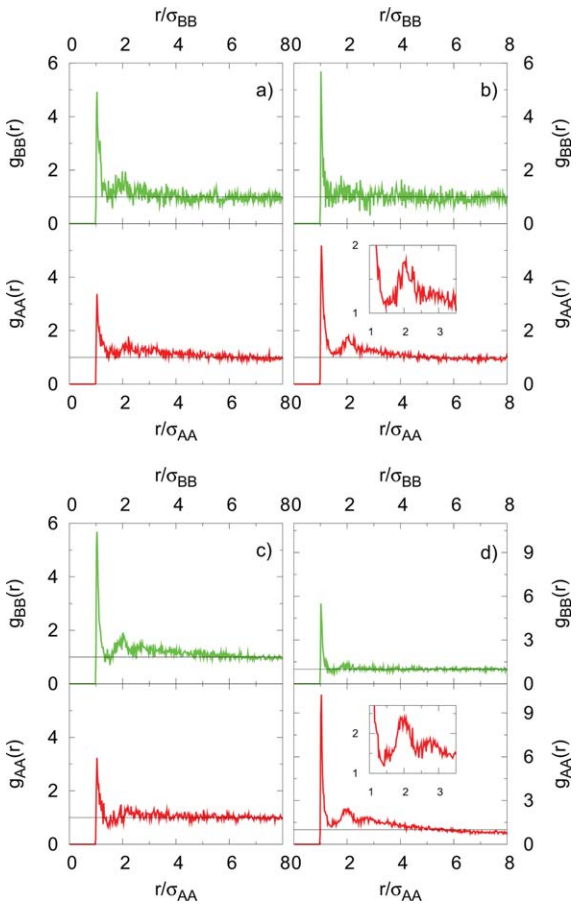

Fig. 4 Radial distribution functions $g_{ii}(r)$ with $i = A, B$ in a slab of thickness $2\sigma_{BB}$ within the middle plane of the simulation box. $Pe_B = 12$ in all cases and a) $N_A = 2N_B$, $Pe_A = 6$; b) $N_A = 2N_B$, $Pe_A = 18$; c) $N_A = N_B$, $Pe_A = 6$; d) $N_A = N_B$, $Pe_A = 18$. Distances are rescaled by appropriate particle diameters σ_{AA} or σ_{BB}. Insets show enlarged area in the region of the second, and in d) the third peak.

resistance when propagating through the solvent (and smaller colloids), and hence they will be slowed down, while the smaller particles are less obstructed. Indeed, in Fig. 2d we see two peaks in the density profile of the lighter, larger particles separated by a peak in the profile of the heavier, smaller particles. This suggests that the smaller particles are penetrating the layers of large particles, (which is in accordance with what we can see in the horizontal plane snapshots in Fig. 3) forcing a quantity of the slower moving particles to flow up together with the solvent. When the larger particles are heavier we see no such effect within the colloidal material (for the parameter range studied here), with the density profiles of both species instead progressing in a very similar fashion. Therefore it would seem that to encourage mixing of particles during sedimentation it would be better to have the smaller particles in the mixture with relatively smaller Peclet numbers.

3.2 Time correlation functions

Having examined the structural properties of the system, we next consider the dynamics of the instability formation process. We calculate the spatial correlations of colloid-velocity fluctuations in the gravity direction within the plane perpendicular to gravity. The correlation functions of the z component are calculated as

$$\frac{C_{ij}(z,r,t)}{k_BT/M_{ij}} = \langle \delta V_i(z,\ 0,\ t)\delta V_j(z,\ r,\ t)\rangle, \qquad (6)$$

where $i, j = A, B$. $\delta V_i(z, r, t) = v_i(z, r, t) - \langle v_i(z, t)\rangle$ is the deviation of the velocity of particle i from the mean velocity in the xy plane at height $z = L_z/2$, at distance r in the xy plane and at time t. We rescale the correlation functions by the corresponding thermal fluctuation strength k_BT/M_{ij}, where $M_{AA} = M_A$, $M_{BB} = M_B$ and $M_{AB} = \sqrt{M_AM_B}$.

The velocity correlations develop in time in such a way that we see pronounced positive correlations at short distances, anti-correlations at larger distances and a final decay to 0 when all the particles have settled onto the bottom wall of the simulation box. The anti-correlation reaching its maximum is an indication that the swirls are fully developed and the distance r at which this occurs is related to the characteristic length of the network-like structure formed. As an illustration of the described behavior, in Fig. 5 we show the r dependence of the $C_{AB}(z, r, t)$ correlation functions for one of the systems studied ($N_A = 2N_B$, $Pe_A = 6$, $Pe_B = 12$) at different times before and after the anti-correlation has reached its maximum.

The results of the calculations of the velocity correlation functions are shown in Fig. 6 and 7 where we can see the time development of the logarithm of the absolute value of $C_{ij}(z, r, t)$ for the mixtures with $N_A = 2N_B$ (Fig. 6) and $N_A = N_B$ (Fig. 7), and Peclet numbers $Pe_A = 6$, 12 and 18, calculated at height $z = L_z/2$. These plots allow us to follow the evolution of the

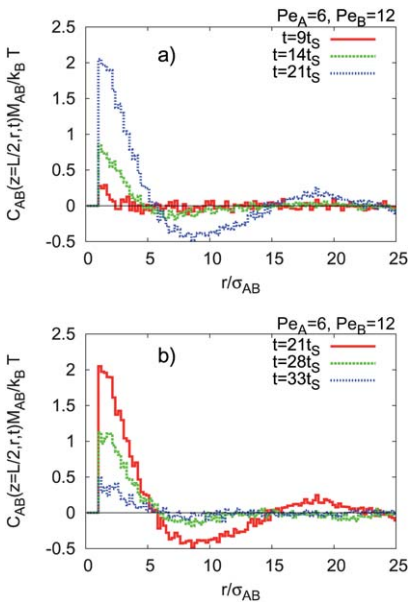

Fig. 5 The time evolution of the r dependence of the spatial velocity correlation functions $C_{AB}(z, r, t)$ for the mixture with $N_A = 2N_B$ particles and Peclet numbers $Pe_A = 6$ and $Pe_B = 12$: a) before the anti-correlation reaches its maximum and b) after the anti-correlation has reached the maximum. The velocity correlations were calculated in the xy plane at $z = L_z/2$ and rescaled by the thermal fluctuation strength k_BT/M_{AB}. The distance r is rescaled by $\sigma_{AB} = (\sigma_{fA} + \sigma_{fB})/2$, and the time t is measured in the units of Stokes time t_S of the larger species.

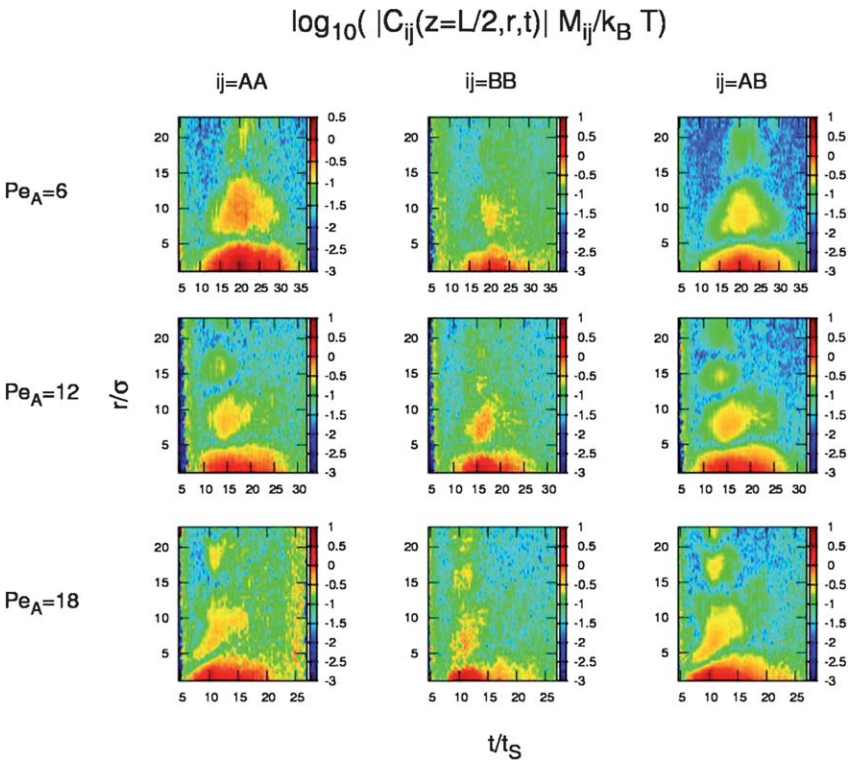

Fig. 6 Spatial velocity correlation functions $C_{ij}(z, r, t)$ for the system with $N_A = 2N_B$. The time evolution of the logarithm of the absolute value of the spatial velocity correlation function $C_{ij}(z, r, t)$, where $ij = AA$, AB or BB, is plotted for the systems with $Pe_B = 12$ and $Pe_A = 6$, 12, 18. The correlation functions were calculated in the xy plane at $z = L_z/2$, and rescaled by the thermal fluctuation strengths k_BT/M_{ij}. Distances r are rescaled by σ, where $\sigma = \sigma_{fA}$ when $ij = AA$, $\sigma = \sigma_{fB}$ when $ij = BB$, or $\sigma_{AB} = (\sigma_{fA} + \sigma_{fB})/2$ when $ij = AB$, and the time t by the Stokes time t_S of species B.

instability by following the time dependence of the characteristic length scale over which the particles are correlated. Looking at larger lengths, we see a second and sometimes even a third characteristic distance region where the particles are also strongly correlated.

As the sedimentation of the system progresses, we can see that the length over which the particles are correlated grows at first for all systems studied. Fig. 6 and 7 show that initially this growth is monotonic in time until the characteristic length reaches a maximum, after which, depending on the Peclet numbers of the particles, it either decreases monotonically or drops slightly before it increases again to a value higher than the first one. This non-monotonic behavior of the characteristic length scale, accompanied by the growing characteristic distances at which the second peaks of the correlation functions appear, is observed for higher Peclet numbers. We note that similar behavior has also been observed for one-component systems[20] indicating that this time dependence of the correlation length is not specific to mixtures but is, instead, an occurrence on the level of the complex fluid.

We also note that the plots presented in Fig. 6 and 7 show that the length over which particle velocities are correlated is larger for the denser system (more particles). This is in accordance with what we also observe in Fig. 3.

3.3 Growth rates

In our simulations we create a configuration suitable for the instability formation by turning the simulation box upside down after the particles have settled on a box wall. In this way the density profile becomes such that the higher layers of the suspension are heavier then the lower ones, forming an interface between the complex fluid, composed of both colloids and the solvent, and the pure solvent.

In the initial regime of the Rayleigh-Taylor instability the interface undulations grow exponentially in time, $\propto \exp(n(k)t)$, where $n(k)$ is the growth rate and $k = (k_x^2 + k_y^2)^{1/2}$ the wave number. We calculate the growth rates both directly from our simulation data and also theoretically *via* the linearized Navier–Stokes equation.[21,22]

Determining when a system leaves the initial linear regime and enters the non-linear regime of the instability can be done by measuring the first and the second density moment in time.[21] The first moment of the density is defined as $\langle z \rangle$, which denotes the center of mass in the z direction of all colloidal particles and quantifies the degree of sedimentation. The second moment of the density, $\sigma_z = \langle z^2 \rangle - \langle z \rangle^2$, quantifies the spread of the colloids in the gravity direction. Fig. 8 shows the first and the second moment as a function of time, rescaled by the height of the simulation box L_z, for the mixtures with $N_A = 2N_B$ and $N_A = N_B$ and varying Pe_A. We distinguish three different regimes in Fig. 8. The initial linear regime, when the undulations of the interface are still small, is identified as the regime where $\langle z \rangle$ slowly decreases and σ_z slowly increases in time. The non-linear regime, when the swirls develop fully, follows, as is indicated by the fast drop in $\langle z \rangle$ and fast increase in σ_z. Finally, both $\langle z \rangle$ and σ_z slowly decrease in time which corresponds to the final settling of the particles at the bottom wall.

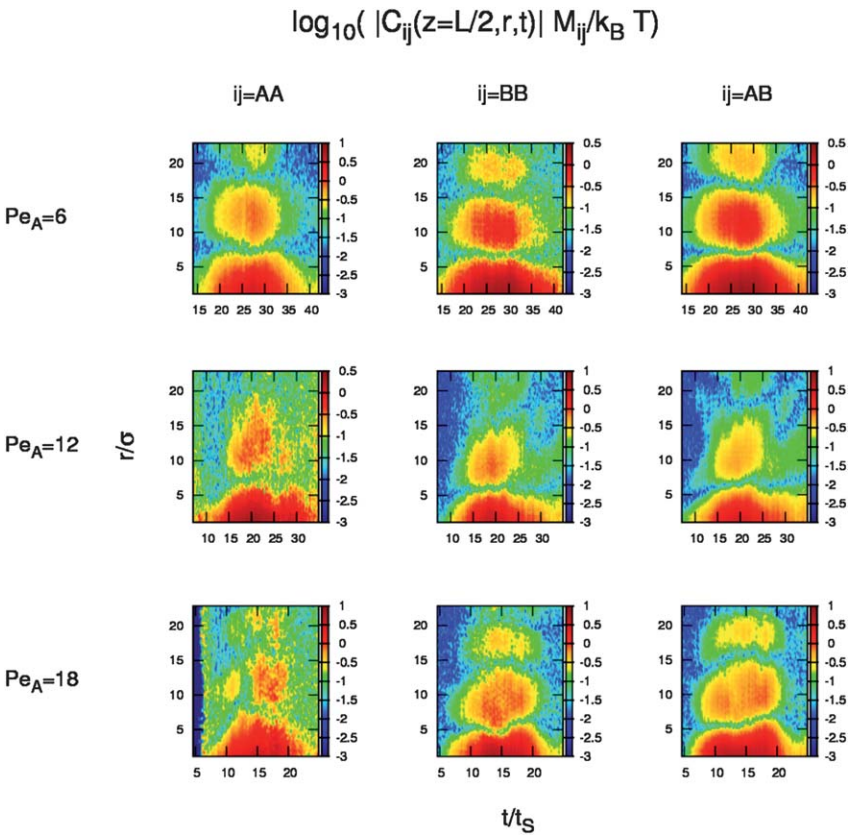

Fig. 7 Spatial velocity correlation functions $C_{ij}(z, r, t)$ for the system with $N_A = N_B$. The time evolution of the logarithm of the absolute value of the spatial velocity correlation function $C_{ij}(z, r, t)$, where $ij = AA$, AB or BB, is plotted for the systems with $Pe_B = 12$ and $Pe_A = 6,12,18$. The correlation functions were calculated in the xy plane at $z = L_z/2$, and rescaled by the thermal fluctuation strengths k_BT/M_{ij}. Distances r are rescaled by σ, where $\sigma = \sigma_{fA}$ when $ij = AA$, $\sigma = \sigma_{fB}$ when $ij = BB$, or $\sigma = (\sigma_{fA} + \sigma_{fB})/2$ when $ij = AB$, and the time t by the Stokes time t_S of species B.

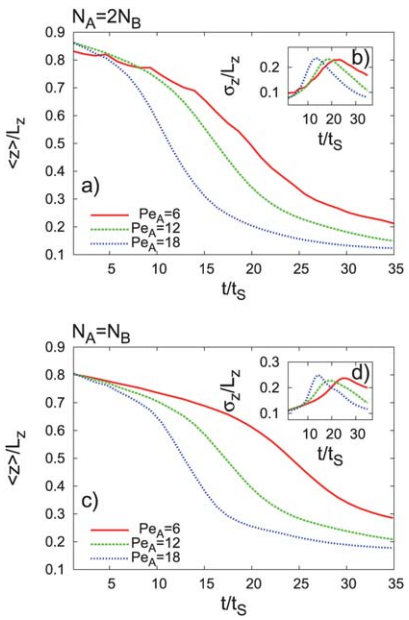

Fig. 8 First moment of the colloidal density $\langle z\rangle/L_z$ and second moment of the colloidal density σ_z/L_z plotted as a function of time for the systems with $Pe_B = 12$, $Pe_A = 6$, 12, 18 and $N_A = 2N_B$: a) and b) and for the system with $N_A = N_B$: c) and d). The time t is measured in units of the Stokes time t_S of the larger species.

From our simulation data, taking into account only the linear regimes, we can calculate the growth rates of the undulations for a range of wave lengths. The results of these calculations are presented in Fig. 9.

To calculate the growth rates theoretically, we require the equations describing the flow of a viscous fluid with varying density. These are the equation of continuity, which expresses the conservation of mass in the system, and the conservation of momentum equation. Using these equations and considering the fluid as incompressible we can write[22]

$$D\left[\left(\rho - \frac{\mu}{n}\left(D^2 - k^2\right)\right)Du_z - \frac{1}{n}D\mu\left(D^2 + k^2\right)u_z\right] + k^2\frac{g}{n^2}D\rho u_z - k^2\left[\rho - \frac{\mu}{n}\left(D^2 - k^2\right)\right]u_z + 2\frac{k^2}{n}D\mu Du_z = 0, \quad (7)$$

where $D = d/d_z$ denotes the derivative with respect to the z coordinate, ρ is the density and μ the viscosity. The velocity u_z must satisfy the boundary conditions $u_z = 0$ and $Du_z = 0$ at $z = 0$ and $z = L_z$. Eqn (7) is a fourth order boundary value problem with variable coefficients, which makes solving it non-trivial. Hence, we must employ numerical techniques. We follow ref. 39 and 40 and divide the fluid into N layers of finite thickness, within which the density and viscosity are treated as constant. In the limit of sufficiently large N eqn (7) can be solved for arbitrary continuous density and viscosity profiles. Treating density and

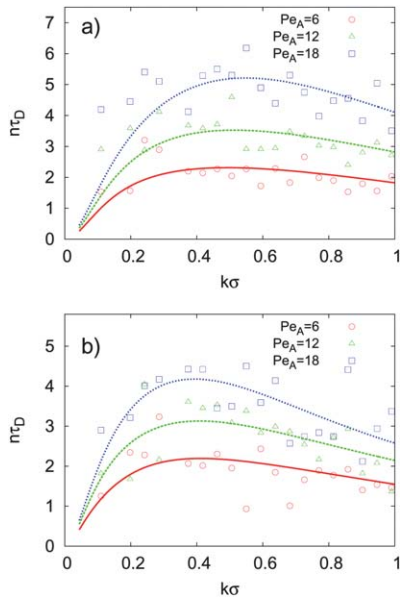

Fig. 9 Growth rates $n\tau_D$ plotted against wave numbers $k\sigma$ of the instability as obtained from the simulations (symbols) and theory (lines). τ_D is the diffusion time of larger colloids (B) and the length σ is taken as the average particle diameter, $\sigma = (\sigma_{AA} + \sigma_{BB})/2$. In all cases $Pe_B = 12$ and we plot the systems with $Pe_A = 6$,12 and 18, for: a) $N_A = 2N_B$ and b) $N_A = N_B$.

viscosity as constants within a layer allows us to formulate an analytical solution within this region. Depending on the specific configuration we define a certain number of layers, and impose boundary conditions for each of them.[22] We differentiate between the two outermost layers that are touching the walls of the simulation box and the inner layers. Each of the surfaces of contact between two fluid layers gives 4 boundary conditions and each of the wall boundaries gives 2 boundary conditions, altogether giving $4N$ equations that we must solve. In the process of solving these equations we obtain a dispersion relation from which we extract the $n(k)$ dependence. Typically we find that we must use $N \sim 20$–30 layers in the calculation.

We use this method to solve eqn (7) for the density profile $\rho(z)$ and the viscosity profile $\mu(z)$ obtained from our simulations. As previously noted, in Fig. 2 we can see that regardless of the initial distributions of the individual particle species within the sediment, the overall initial density profiles resemble those of a one-component system[19] - in the sample preparation process the colloidal material simply settles on the bottom wall of the simulation box to minimize the potential energy. This suggests that from a macroscopic perspective we should be able to analyze the instability in terms of the instability of a complex fluid described by the overall density and viscosity profiles, rather than those of the individual species. Based on the colloidal packing fraction profiles, which we obtain from the equilibrated simulations, we calculate the mass density as $\rho(z) = \phi_A(z)\rho_A + \phi_B(z)\rho_B + (1 - \phi_A(z) - \phi_B(z))\rho_f$, where $\phi_A(z)$ and $\phi_B(z)$ are the colloidal packing fraction profiles and ρ_A, ρ_B and ρ_f are mass densities of species A, B and the fluid respectively.

Calculating the viscosity from the simulation data, *i.e.* as a function of the particle packing fraction, turns out to be surprisingly difficult for our systems. Since the suspensions we are studying are not dilute, most of the standard methods (see *e.g.* ref. 41) are not valid. Instead we use a viscosity description proposed by Mendoza and Santamaria-Holek[41] which is valid for concentrated suspensions of mono- and poly-disperse colloidal particles. With the density and viscosity profiles calculated we extract the $n(k)$ dependence from eqn (7) and plot this in Fig. 9 for each of our systems. We note that it is also necessary to include a correction of the form $n^*(k) = n(k) - (D_A + D_B)k^2$ which takes into account the effects of particle diffusion,[21] where D_A and D_B are the diffusion constants of particles A and B respectively.

We first note that for all systems studied we find excellent qualitative and quantitative agreement between the theoretical predictions and the simulation results. We observe that for both mixtures ($N_A = 2N_B$ and $N_A = N_B$) the growth rates reach their maxima at finite values of the wave number k. The wave lengths corresponding to the wave numbers for which the maxima are reached are the initially fastest growing wave lengths. In Fig. 9 it can also be seen that the growth rates are larger for systems with larger Peclet numbers of species A. This indicates that the interface undulations, which develop as a consequence of the instability, develop faster for systems with higher Pe_A. The interface between the colloid-rich and the pure solvent regions in these systems deforms faster and allows the fluid to penetrate the colloidal layer sooner. This leads to faster formation of the swirls that facilitate the fast sedimentation of the colloidal material (see also Fig. 8), until the system reaches a stable configuration.

4 Conclusions

Using a computer simulation technique that incorporates both long ranged hydrodynamic interactions between particles and Brownian forces acting on them, we have studied the sedimentation of binary mixtures of hard sphere-like colloids confined to a slit on the particle-scale level. Initial configurations which are vertically inhomogeneous in such a way that a heavy colloid-fluid layer is placed above pure solvent, are not stable with respect to gravity and hence result in the formation of a Rayleigh-Taylor-like instability. In this paper, we have investigated the effects of changing the strength of the gravitational drive of one of the species, by changing its Peclet number, on the formation and development of the instability, and on the properties of the transient network-like structures that form during the sedimentation. By keeping the Peclet number of the larger particles fixed and changing that of the smaller particles we have simulated a range of relative Peclet number scenarios for two different mixtures.

We find that the organization of the particles within the droplets formed during the sedimentation depends substantially on the relative Peclet numbers and less so on the composition of the mixture. For mixtures in which the smaller particles have relatively larger Peclet numbers dense droplets, with smaller particles mostly on the inside and larger particles mostly on the outside, form. For mixtures in which the smaller particles have relatively smaller Peclet numbers we again see the formation of droplets, but without any specific organization of particles within them. Our results indicate that when the smaller particles have larger Peclet numbers, within the instability they cluster to

facilitate forcing their way through the lower layers of the suspension, causing a backflow of larger colloids together with the solvent. Therefore, to maintain a mixed sample throughout the sedimentation process it would be desirable to have smaller colloids with a relatively lower Peclet number.

The calculations of the spatial velocity correlation functions allow us to follow the development of the instability in time by following the changes of the length scale over which the particle velocities are correlated. As the instability develops the correlation length increases, showing the existence of length scales over which the particle velocities are correlated, followed by regions of anti-correlation, and then by regions of correlation again at even larger distances. The distances at which we see anti-correlations correspond to the average distances between regions of particles moving in opposite directions, giving us an indication of the sizes of the droplets. Also, for larger Peclet numbers we see that the correlation lengths no longer grow monotonically and that the higher the Peclet number, the faster the development of the instability. For denser systems, *i.e.* more particles in the slit, we see that the characteristic dimensions of colloidal droplets made of particles with correlated velocities are larger. We also find that the second correlation regions are more pronounced for these denser systems, indicating that the droplets are more compact.

Finally, we have calculated the growth rates of the unstable modes both from our simulation data and *via* a linear stability analysis, finding good qualitative and quantitative agreement. We find that the instability behavior depends only on the macroscopic properties of the complex fluid and not on the specific distributions of colloids within the mixture. Our results show the existence of a wave length of fastest growth for each system studied. Increasing the Peclet number of the smaller particles leads to the overall increase in the magnitude of the growth rates, *i.e.* the interface between the colloid-rich and pure solvent regions deforms faster. We also find that the wave numbers corresponding to fastest growing wave lengths increase with the Peclet number.

In conclusion, we find that the key parameter for the manipulation of distribution of colloids within the Rayleigh-Taylor-like instabilities in binary colloidal mixtures is the relative magnitude of the Peclet numbers of the particle species, while the instability of the complex fluid itself can be described by overall density and viscosity profiles. In an experimental system these parameters could be controlled by fabricating colloids from different materials and adjusting the solvent density.

MD acknowledges financial support from an NWO-VICI grant. We thank A. Wysocki for stimulating discussions.

References

1 U. Gasser, *J. Phys.: Condens. Matter*, 2009, **21**, 203101.
2 C. M. Soukoulis, *Photonic Crystals and Light Localization in the 21st Century*, Kluwer Academic Publishers, 2001.
3 M. Maldovan, C. K. Ullal, W. C. Carter and E. L. Thomas, *Nat. Mater.*, 2003, **2**, 664.
4 A. Moroz, *Phys. Rev. B: Condens. Matter*, 2002, **66**, 115109.
5 A. J. Garcia-Adeva, *New J. Phys.*, 2006, **8**, 86.
6 T. Ngo, C. M. Liddell, M. Ghebrebrhan and J. D. Joannopoulos, *Appl. Phys. Lett.*, 2006, **88**, 241920.
7 W. B. Pearson, *The Crystal Chemistry and Physics of Metals and Alloys*, Elsevier, New York, 1972.
8 A.-P. Hynninen, J. H. J. Thijssen, E. C. M. Vermolen, M. Dijkstra and A. van Blaaderen, *Nat. Mater.*, 2007, **6**, 202.
9 A.-P. Hynninen, L. Filion and M. Dijkstra, *J. Chem. Phys.*, 2009, **131**, 064902.
10 E. V. Shevchenko, D. V. Talapin, N. A. Kotov, S. O'Brien and C. B. Murray, *Nature*, 2006, **439**, 55.
11 G. H. Ma, T. Fukutomi and N. Morone, *J. Colloid Interface Sci.*, 1994, **168**, 393.
12 S. Yoshimura and S. Hachisu, *Prog. Colloid Polym. Sci.*, 1983, **68**, 59.
13 P. Bartlett, R. H. Ottewill and P. N. Pusey, *Phys. Rev. Lett.*, 1992, **68**, 3801.
14 E. C. M. Vermolen, PhD thesis, Utrecht University, 2008.
15 J. S. Turner, *Annu. Rev. Fluid Mech.*, 1974, **6**, 37.
16 D. Velegol, S. Shori and C. E. Snyder, *Ind. Eng. Chem. Res.*, 2009, **48**, 2414.
17 H. A. Jerri, W. P. Sheehan, C. E. Snyder and D. Velegol, *Langmuir*, 2010, **26**, 4725.
18 C. Royall, J. Dzubiella, M. Schmidt and A. van Blaaderen, *Phys. Rev. Lett.*, 2007, **98**, 188304.
19 J. T. Padding and A. A. Louis, *Phys. Rev. E: Stat., Nonlinear, Soft Matter Phys.*, 2008, **77**, 011402.
20 A. Wysocki, C. P. Royall, R. G. Winkler, G. Gompper, H. Tanaka, A. van Blaaderen and H. Lowen, *Faraday Discuss.*, 2010, **144**, 245–252.
21 A. Wysocki, C. P. Royall, R. G. Winkler, G. Gompper, H. Tanaka, A. van Blaaderen and H. Lowen, *Soft Matter*, 2009, **5**, 1340–1344.
22 S. Chandrasekhar, *Hydrodynamic and Hydromagnetic Stability*, Oxford University Press, Oxford, 1961.
23 J. T. Padding and A. A. Louis, *Phys. Rev. Lett.*, 2004, **93**, 220601.
24 J. K. G. Dhont, *An Introduction to Dynamics of Colloids*, Elsevier, Amsterdam, 1996.
25 A. Malevanets and R. Kapral, *J. Chem. Phys.*, 1999, **110**, 8605.
26 A. Moncho-Jordá, A. A. Louis and J. T. Padding, *Phys. Rev. Lett.*, 2010, **104**, 068301.
27 M. Hecht, J. Harting, T. Ihle and H. J. Herrmann, *Phys. Rev. E: Stat., Nonlinear, Soft Matter Phys.*, 2005, **72**, 011408.
28 M. Hecht, J. Harting, M. Bier, J. Reinshagen and H. J. Herrmann, *Phys. Rev. E: Stat., Nonlinear, Soft Matter Phys.*, 2006, **74**, 021403.
29 M. Hecht, J. Harting and H. J. Herrmann, *Phys. Rev. E: Stat., Nonlinear, Soft Matter Phys.*, 2007, **75**, 051404.
30 S. H. Lee and R. Kapral, *J. Chem. Phys.*, 2006, **124**, 214901.
31 M. Ripoll, R. G. Winkler and G. Gompper, *Phys. Rev. Lett.*, 2006, **96**, 188302.
32 K. Mussawisade, M. Ripoll, R. G. Winkler and G. Gompper, *J. Chem. Phys.*, 2005, **123**, 144905.
33 H. Noguchi and G. Gompper, *Phys. Rev. Lett.*, 2004, **93**, 258102.
34 J. L. McWhirter, H. Noguchi and G. Gompper, *Proc. Natl. Acad. Sci. U. S. A.*, 2009, **106**, 6039–6043.
35 H. Noguchi and G. Gompper, *J. Chem. Phys.*, 2006, **125**, 164908.
36 J. T. Padding and A. A. Louis, *Phys. Rev. E: Stat., Nonlinear, Soft Matter Phys.*, 2006, **74**, 031402.
37 T. Ihle and D. M. Kroll, *Phys. Rev. E: Stat. Phys., Plasmas, Fluids, Relat. Interdiscip. Top.*, 2001, **63**, 020201.
38 D. Frenkel and B. Smit, *Understanding Molecular Simulation*, Academic Press, London, 2002.
39 K. O. Mikaelian, *Phys. Rev. Lett.*, 1982, **48**, 1365.
40 K. O. Mikaelian, *Phys. Rev. E: Stat. Phys., Plasmas, Fluids, Relat. Interdiscip. Top.*, 1996, **54**, 3676.
41 C. I. Mendoza and I. Santamaría-Holek, *J. Chem. Phys.*, 2009, **130**, 044904.

